HADRONIC FINAL STATES IN PHOTOPRODUCTION AT THE ep COLLIDER HERA

J. RIEDLBERGER
(FOR THE H1 COLLABORATION)
Institut für Teilchenphysik, Eidgenössische Technische Hochschule Zürich, CH 8093 Zürich, Switzerland

ABSTRACT

Photoproduction events, observed in ep collisions show a hard component. Using the kinematics of the partons involved, the structure of the photon is extracted and its gluon content is found. Diffractive events are studied showing a hard scattering too. A preliminary analysis of final state pion interferometry for photoproduction events leads to $r_{BE} = 1.04 \pm 0.04_{stat} \pm 0.1_{sys} fm$ and $\lambda = 0.54 \pm 0.04_{stat} \pm 0.07_{sys}$, similar to values observed in meson–proton collisions.

1 Introduction

At the first electron–proton collider HERA, protons are accelerated to an energy of 820 GeV to collide on 27.5 GeV electrons. Since the commissioning in summer 1992 two experiments H1[1] and ZEUS[2] measure ep scattering at a center of mass energy of 296 GeV. The incoming lepton interacts with the hadron, or parts of it, via the exchange of a gauge boson: γ, Z^0 or $W^{\pm}$. Depending on the nature of the gauge boson, in case of a W exchange a neutrino (charged current) or γ, Z^0 exchange an electron (neutral current) is observed in the final state. The kinematics can be described as a two particle scattering, if all products of the final state except the lepton are grouped together (fig. 1). For fixed incoming proton and electron energies the kinematics is determined through the measurement of one of the four–vectors of the final state, i.e. the electron or the hadronic system. The negative four–momentum transfer squared from the initial to the scattered lepton is defined as $Q^2 = -q^2 = -(k-k')^2$. The Bjorken x is the fraction of proton momentum of a massless parton interacting by an elastic process with the electron. The energy fraction transferred to the proton from the electron in the proton rest frame is called y. At fixed center of mass energy $\sqrt{s} = \sqrt{4E_eE_p} = 296GeV$ these three Lorentz invariant quanitities are related through $Q^2 = xys$.

Using the energy and angle measurement of the electron only, the kinematic variables (see fig. 1) can be determined by

$$Q^2 = 4E_eE_e'cos^2(\frac{\theta_e}{2}) \qquad\qquad y_e = 1 - \frac{E_e'}{E_e}sin^2(\frac{\theta_e}{2}). \tag{1}$$

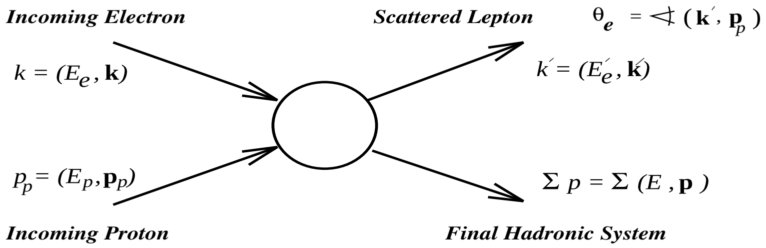

Figure 1: Definition of the kinematic quantities in ep scattering.

The usage of quantities determined from the hadronic final state system is favorable at low y_e, as $\frac{dy_e}{y_e} = \frac{1}{y_e}$ yields to a big factor in the error propagation and for the kinematic region, where radiative order corrections for the electrons are necessary. In this case the incoming electron may be different from the interacting electron, entering the scatter process. Using the approximation of Jacquet – Blondel [3], y can also be determined as

$$y_{JB} = \frac{\sum_{Hadrons}(E - p_z)}{2E_e}. \tag{2}$$

In this equation, the non measured fraction of the hadronic system, which disappears in the beampipe in the proton direction, contributes only marginally to the sum.

The time scales of the initial scattering process with the electron and the subsequent evolution of the hadronic system decouples both processes. Using the kinematics of the measured electron, ep scattering provides an ideal system for fragmentation studies of hadronic systems.

2 Photoproduction

2.1 Processes with almost Real Photons

The invariant mass of the exchanged particle is given by the quantity Q^2. For interactions with $Q^2 \sim 0$ the virtually exchanged photon is almost on its mass shell. These interactions are called (almost) real photoproduction processes.

Inserting $Q^2 \sim 0$ in equation 1 leads to scattering angles of about 180 degrees with respect to the outgoing proton direction. Consequently, in photoproduction the scattered electron escapes the detection in the main detector through the beampipe. From the experimental point of view there are two classes of photoproduction events [4].

Tagged γ p events : In this case the scattered electron is detected in a small angle calorimeter (e–tagger) outside of the main experiment. In coincidence with another small calorimeter (Photon–Tagger), this detector is also used to measure Bremsstrahlung processes $ep \rightarrow e'\gamma p$. With the help of the precisely known cross section [5] of Bremsstrahlung events the luminosity of HERA at H1 is determined.

In ep scattering the observation of the scattered electron significantly discriminates against background events. Furthermore the knowledge of the energy of the scattered electron allows a determination of the mean value of the center of mass energy $W_{\gamma p} = \sqrt{s_{\gamma p}} \sim 195 GeV$ for photoproduction events. The increased center of mass energy at HERA, compared to previous experiments opens a new kinematic regime of photon hadron scattering.

untagged γ p events : As no information of the scattered electron is available, another criterion to discriminate against beamgas background events has to be applied. In general the z-vertex information reduces the bulk of background, however, for rejecting proton restgas interaction within the interaction region another cut has to be made. The measurement of $\sum(E - p_z)$ of all observed scattering products is proportional to y$_{JB}$ (equation 2, as the electron is not detected) which yields the value $2E_\gamma$ for photoproduction events, while for proton restgas events the value $\sum(E-p_z) = m_A$ (m_A is the mass of the restgas nucleus) is expected. A cut on the kinematical variable y_{JB} therefore purifies the data sample. The experimental verification of this method is achieved by the analysis of events, originating from HERA machine bunches, which have no corresponding electron bunch when they cross the interaction region. By selecting these events a pure proton restgas sample can be obtained and compared to genuine e–p scattering events.

For special photoproduction events, like $\gamma p \rightarrow \rho p$, $\gamma p \rightarrow J/\psi$, the event kinematics can be reconstructed by their final state [6].

2.2 Experimental Classification of Photoproduction Events

The main fraction of the γp cross section can be described by phenomenological non-perturbative models [8]. These **soft processes** are characterized by a differential p_t cross section with an exponential fall off. Figure 2 (left) shows the p_t distribution for charged particles [7] in comparison with γp events at lower CMS energy and with hadron-hadron scattering events at the same energy. An additional component at high p_t is clearly visible. Deviations from the exponential tail are taken as an evidence for

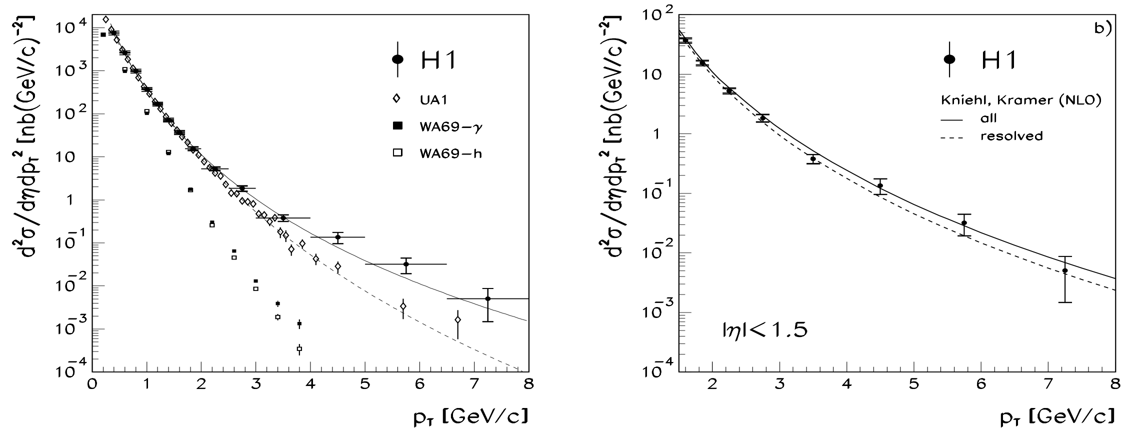

Figure 2: The inclusive ep cross section for charged particles in tagged photoproduction: Left: Shape comparison with UA1 $\bar{p}p$ data at $W_{\gamma p} \sim 200 GeV$ and WA69 for γp and hadron–proton data at $W_{\gamma p} \sim 18 GeV$. Right: Comparison with an analytic calculation.

the existence of hard processes.

In **hard scattering processes**, a perturbative description of the initial scattering of the photon (or parts of it) with a parton in the proton is applied. The hard contributions to the total cross section are classified in two groups (fig. 3): In **Direct Processes** the whole photon, as a gauge particle interacts, leading to **QCD Compton** or **Photon Gluon Fusion** processes. On the other hand only a part of the photon might scatter in the **Resolved Processes**. In this case, the photon will fluctuate into a bound $q\bar{q}$ pair (**Vector Dominance Model**) [9] or split to an unbound pair (**Anomalous Component**). The experimental signature of the classification of these events is the measurement of the photon remnant. Figure 2 (right) shows the high energetic tail of the p_t distribution in comparison with an analytic calculation. Additional to the resolved component a direct component is necessary to describe the data.

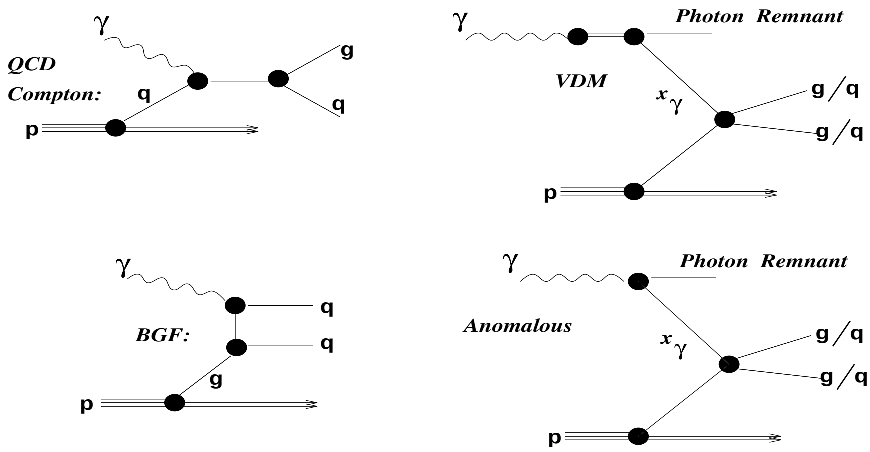

Figure 3: Graphs for initial hard scattering γp processes. Left: QCD diagrams of direct processes. Right: Resolved processes for an hadronic structure of the photon, leading to a photon remnant

At hadron-hadron collisions at the same energy a nonexponential behavior of the p_t spectrum is also observed (fig. 2 left). However, the direct processes additionally increase the hard contribution for γp processes at HERA [10].

2.3 The Structure of the Photon

Another powerful proof for the existence of hard processes is the observation of jets [11,12], which justifies the underlying initial hard process. The energy flow, measured with the calorimeter in the azimuth (φ) – pseudorapidity ($\eta = -\ln(\tan\frac{\theta}{2})$) plane is analyzed. In analogy to hadron–hadron scattering a cone algorithm [13] is applied: clusters with a transverse energy bigger than 7 GeV within a Radius $R = \sqrt{\Delta\eta^2 + \Delta\varphi^2} = 1$ are identified as jets.

Hard Processes, as depicted in figure 3 have at least two jets. They are called 2+1 jet events, taking the non- or only fractionally measured proton remnant into account.

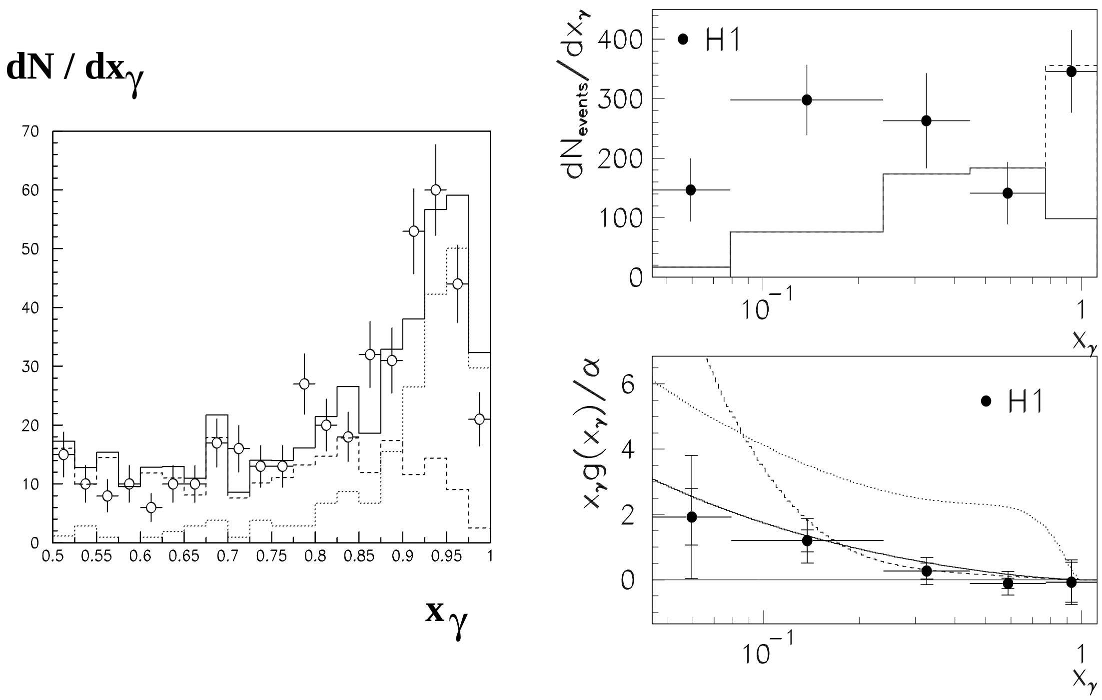

Figure 4: Left : x_γ^{rec}-distribution (circles) for untagged events compared with PYTHIA. Dotted : direct component, dashed: resolved and full histogram: sum of both. Right Top: x_γ^{true}-distribution for e-tagged data in comparison with a PYTHIA prediction using a quark structure of the photon only. Only statistical errors are shown. Right Bottom: Measured gluon density in the photon for e-tagged data, compared with the GRV-LO (full) and two LAC (dotted) distributions.

For extracting properties of the hard scattering process the parton kinematics is assigned to the jet kinematics. The validity of this assignment is checked with Monte Carlo Calculations. The momentum fraction x_γ of a parton in the photon is calculated using

$$x_\gamma = \frac{E_{parton}}{E_\gamma} \approx \frac{E_t^{jet1} e^{-\eta^{jet1}} + E_t^{jet2} e^{-\eta^{jet2}}}{2 \cdot E_\gamma} \approx \frac{\sum_{Jets}(E - p_z)}{2 \cdot E_\gamma} \qquad (3)$$

Figure 4 (left) shows the x_γ distribution of untagged photoproduction events. A Monte Carlo calculation for resolved processes, folded with the detector acceptance cannot explain the enhancement at large x_γ, indicating the existence of direct processes. Here the photon energy required for equation 3 is calculated using

$$2 \cdot E_\gamma = 2 \cdot \sum_{Hadrons} (E - p_z) \qquad (4)$$

For direct processes, all of the photon energy is used for the production of two jets and no remnant is observed. Therefore no additional hadrons are observed outside the jet and inserting E_γ into equation 3 yields the value one. In this method some systematic errors, like uncertainties in the calibration, cancel.

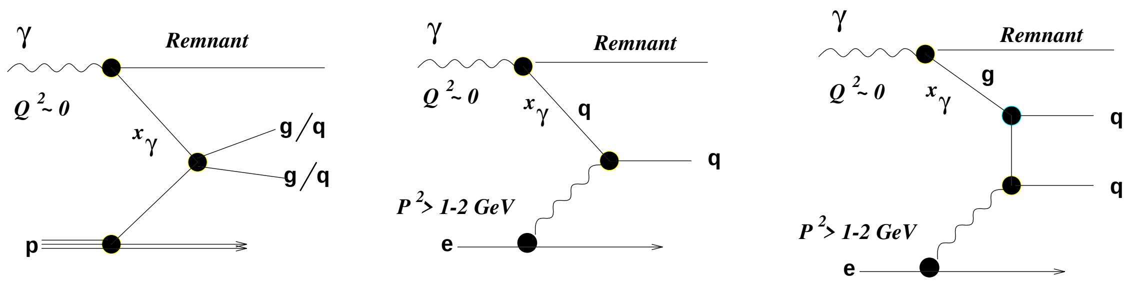

Figure 5: Graphs for initial hard scattering γp processes. Left: Probing the photon at HERA. Center and Right: Diagrams for photon–photon collisions at LEP

The bulk of 2-jet γp events are due to resolved processes. To determine the hadronic structure of the photon, tagged γp events are used. A comparison with a PYTHIA [14] Monte Carlo calculation shows a poor description of the energy flow at large pseudo rapidities, e.g. of energy measurements close to the outgoing proton direction. A substantial improvement of the description was obtained by including the multiple interaction option in the MC generation. However, for extracting jet energies a pedestal subtraction, measured in the sidebins, was applied to overcome these different jet shapes. Jets within the pseudo–rapidity interval $-0.2 \leq \eta_{jet} \leq 2.5$ gave access to the momentum fraction of partons in the range $0.03 \leq x_\gamma \leq 1.$. The energy of the photon is determined by the measured energy of the scattered electron: $E_\gamma = E_e - E_{e'}$. In the next step the momentum fraction x_γ^{true} of the parton in the photon is extracted with an unfolding procedure from the measured x_γ . Figure 4 (right top) shows the resulting x_γ^{true} distribution and a PYTHIA prediction, which was tuned to LEP data and therefore is dominated by the quark structure of the photon only. An enhancement at low x_γ^{true} which is attributed to a gluon contribution in the photon is observed. The unfolded x_γ^{true} distribution can be compared with two photon interactions, observed at e^+e^- experiments [15,16]. Here one (quasi) real photon is probed by a virtual photon. Figure 5 illustrates the difference of probing a photon with a quark at HERA or probing it with a virtual photon at LEP. At LEP the quark content of the photon to be probed dominates, hence the virtual photon does not couple directly to gluons (see fig. 5 center). Under these assumptions, the direct contribution (from MC) [17,18] and the quark distribution (from LEP) can be subtracted, allowing an extraction of the gluon density in the photon.(Fig. 4 right bottom)

In summary we observe hard processes with jets in γp events at $\sqrt{s_\gamma} = 195 GeV$ with both a direct and a resolved component. The latter allows to determine the hadronic structure of the photon where a gluon contribution, as expected, is found.

2.4 Soft Processes

The photon can fluctuate into a vector meson with the same quantum numbers. The majority of the events show the same soft features as observed in hadron–hadron collisions (e.g. charged multiplicities). A phenomenological description with the

Vector Dominance Model describes the total cross section up to the CMS energy region of HERA. The processes involved are of non perturbative nature and not calculable in QCD. However, from the experimental point of view two big classes of events can be defined. The main fraction of events (64.0 % [19]) are following a **non–diffractive** signature (fig. 6). If there is no exchange of quantum numbers, but only of energy and momentum, the events are called **diffractive**. In this case, both (**double dissociation**) or one (**single dissociation**) of the scattering particles may fragment into multiparticle clusters (23.3% [19]). If no dissociation is observed **elastic** scattering of a Vector Meson on the proton occurred (12.7 % [19]).

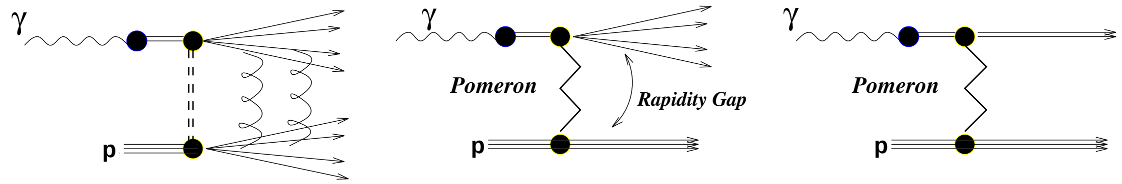

Figure 6: Graphs for soft scattering γp processes. Left: Non diffractive processes with color flow in the final states Center: Single Diffractive with single Dissociation (Pomeron exchange) Right: Elastic diffractive scattering

The experimental signature of diffractive events are rapidity gaps. As there is no color flow between the scattered objects, a certain region in the rapidity spectrum will not be populated by final state particles. Striking are the events with no or only small mass proton dissociation. In this case, no particles are observed in the forward hemisphere, e.g. the region around the outgoing proton direction. A significant detector originating variable to separate these events is η_{max}, the largest measured value of pseudorapidity in an event. Small values of η_{max} mean that there is no activity in the large η region of the detector, beeing the direction of the outgoing proton. Hence a gap between final states of the proton (remnant) and the scattered

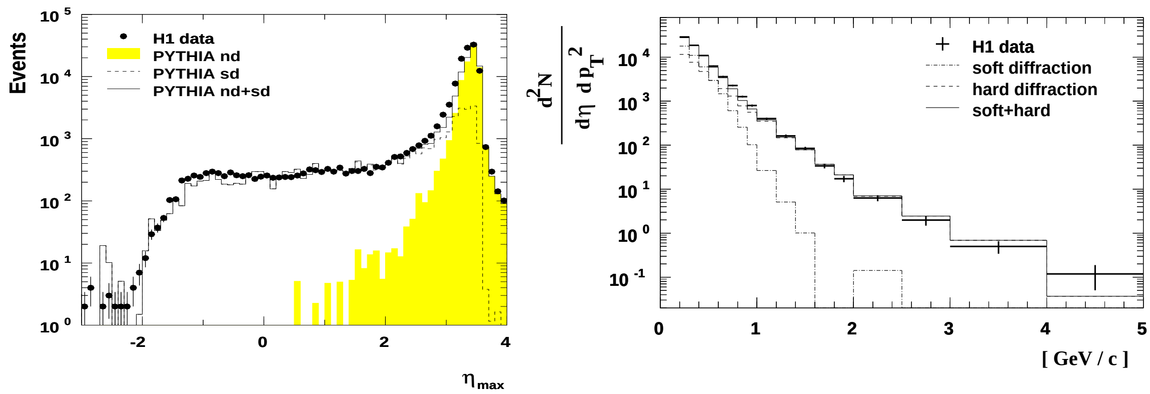

Figure 7: Left: Maximum pseudo-rapidity η_{max} distribution in tagged γp events in comparison with PYTHIA Monte Carlo simulations. nd: non-diffractive, sd: single diffractive contribution. Right: Transverse momentum distribution of charged particles for events with large pseudo-rapidity gap (η_{max} <1.5)

vector meson is observed.

H1 [20] analysed the η_{max} distribution for tagged events. Fig. 7 (left) shows that the main fraction of events with large η_{max} values is well described by a non–diffractive Monte Carlo, however, a non exponential tail to small η_{max} values is visible. The single diffractive model gives a good description for the shoulder at η_{max} smaller than 2.

The exchange of energy and momentum can be assigned to an object, called the Pomeron [21]. The clear separation of diffractive events by means of a η_{max} cut raise the possibility to study the structure of the Pomeron. as a hadronic system. High mass diffractive dissociation is found to exhibit a large p_t tail and even the production of jets. Figure 7 (right) shows the p_t spectrum of charged particles for events with $\eta_{max} \leq 1.5$. A similar high p_t tail as in the overall photoproduction p_t spectrum is visible. The addition of a hard diffractive component (POMPYT) [22] to the soft diffractive part in the Monte Carlo calculation describes this non–exponential tail. At H1 in this photoproduction subsample also jets are observed. Using the parton densities in the photon, the analysis of diffractive events with jets will allow a determination of the Pomeron structure.

3 Bose – Einstein Analysis in γp

An important aspect of the fragmentation of quarks is the formation of the final state mesons. Following a traditional point of view the initial hard process leading to colored objects is decoupled from the subsequent hadronization. The analysis of meson pair correlations or Bose – Einstein correlations as they are refered to in the literature (see e. g. [23]) provides one of the means to test this idea experimentally. In such an analysis one calculates differences in the four–momentum components for pairs of like signed charged pions or kaons and then compares their distributions for different event classes to reference spectra from uncorrelated pairs, typically constructed by looking at pairs of bosons with opposite charge or taken from different events. Since the discovery of these correlations 35 years ago analyses of many experiments consistently showed an enhancement of the rates for small relative momenta, which has been interpreted in different ways. We briefly recall the general ideas behind the two principal lines of arguments here [23], before we list our own results and compare them with existing ones from other high energy processes.

The first approach follows the interpretation of second order intensity correlations (Hanbury Brown Twiss effect) used in optics to determine the radii of stellar light sources and prevails mainly in the analysis of heavy ion collisions. The extent of the enhancement in momentum space simply is given by the Fourier transform of the size of the pion source. Inherent to this interpretation is the assumption of spatially distributed, independent boson emitters (from independent nucleon nucleon collisisons or radiating atoms) with random relative phases, i. e. incoherent sources. The amount of chaoticity of the source can in this picture directly deduced from the value of the parameter λ in equation 5.

Alternatively the enhancement arises naturally from the symmetrization of the final state wave function for the pair of identical bosons, which favors overlapping states for the two particles in energy and momentum. The extent of the enhancemant can again be linked to the space-time development of the source. In the string model for mesons contained in quark initiated jets [24], the particles are produced along a hyperbola $t^2 - x^2 = \tau^2$ (x, t is the space-time production point of the particle and τ the time for the particle freeze out). The non–coherent phases arise naturally through their world-sheet history (e.g. their $\Delta(t, x)$ difference). The parameters extracted from the pion-correlation analysis are related to the string tension. Within this ansatz one expects a difference between high energy elementary particle reactions and heavy ion collisions.

In heavy ion collisions [25] a twodimensional analysis of the pair correlation in the variables $q = |\vec{p}_1 - \vec{p}_2|$ and $q_0 = E_1 - E_2$ show a decrease of the effect along both axes, as one expects from classical 2^{nd} order interference of a static fireball [26]. In elementary particle collisions an increase along the diagonal $q_0 = q$ is observed, which leads the experimenters to preferentially present the correlation in the variable $Q^2_{BE} = (p_1 - p_2)^2 = (\vec{p}_1 - \vec{p}_2)^2 - (E_1 - E_2)^2$. The (hidden) light cone features of the model may make this the natural choice, however, as q and q_0 are not Lorentz-frame invariant, no definite experimental conclusions from the comparison of the two methods have been drawn so far.

In this analysis we also use the variable $Q^2_{BE} = (p_1 - p_2)^2 = m^2_{12} - 4m^2_\pi$. This quantity is Lorentz invariant and allows comparisons with other experiments independent of the reference frame, as long as one does not spoil this argument by splitting the event sample into different bins in pseudorapidity.

At H1 a preliminary Bose-Einstein analysis of all events from an minumum bias photoproduction sample was performed. Tracks, measured by the two-segmented central jet chamber [27] are selected. Only long tracks defined as being measured in

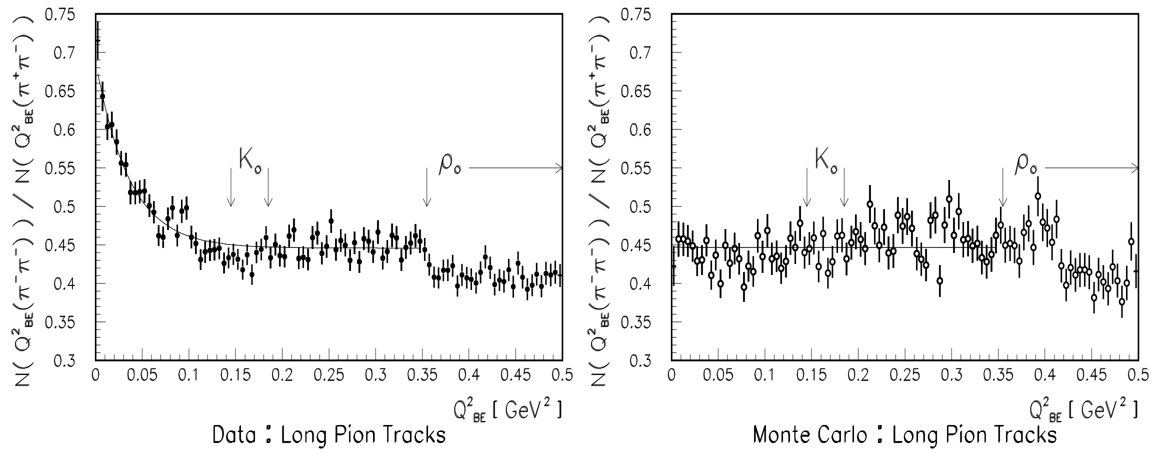

Figure 8: Bose Einstein Correlation for photoproduction events at H1. Left : Data, Right : Monte Carlo

Experiment	λ	Radius [fm]	Ref.
pp at E766	0.44 ± 0.1	0.98 ± 0.12	[28]
pp at NA23	0.38 ± 0.06	0.91 ± 0.10	[29]
pp at NA27	0.37 ± 0.02	1.16 ± 0.06	[30]
$p\bar{p}$ UA1 at $\sqrt{s} = 630GeV$	0.17 ± 0.03	0.74 ± 0.03	[31]
$p\bar{p}$ UA1 at $\sqrt{s} = 900GeV$	0.19 ± 0.03	0.81 ± 0.04	[31]
$p\bar{p}$ at E735	0.40 ± 0.02	0.86 ± 0.04	[32]
e^+e^- MARK2 at SPEAR J/ψ	1.00 ± 0.11	0.81 ± 0.07	[33]
e^+e^- MARK2 $\sqrt{s} = 4.1 - 6.7GeV$	0.66 ± 0.09	0.71 ± 0.07	[33]
e^+e^- ARGUS at Y_{1s}	0.72 ± 0.09	0.77 ± 0.08	[34]
e^+e^- ARGUS at $\sqrt{s} = 9.4 - 10.5GeV$	1.11 ± 0.20	1.13 ± 0.14	[34]
e^+e^- at TPC	0.61 ± 0.11	0.65 ± 0.09	[35]
e^+e^- MARK2 at PEP gg	0.87 ± 0.14	0.84 ± 0.11	[33]
e^+e^- MARK2 at PEP qq	0.31 ± 0.04	0.88 ± 0.09	[33]
e^+e^- at TASSO	0.31 ± 0.04	0.88 ± 0.09	[36]
e^+e^- at OPAL	0.87 ± 0.17	0.93 ± 0.17	[37]
e^+e^- at DELPHI	0.40 ± 0.08	0.62 ± 0.24	[38]
e^+e^- at ALEPH	0.51 ± 0.15	0.65 ± 0.20	[39]
νN at WA21, WA25, WA59 and E180	0.80 ± 0.20	0.61 ± 0.19	[40]
νD_2 at WA25	0.57 ± 0.19	0.43 ± 0.12	[41]
μp at EMC–NA9	0.84 ± 0.03	1.08 ± 0.10	[42]
ν Freon at SKAT	0.95 ± 0.18	0.91 ± 0.24	[43]
πp at 200 GeV	0.8 ± 0.1	0.67 ± 0.07	[44]
πp and Kp at NA22	0.38 ± 0.01	0.83 ± 0.02	[45]

Table 1: Bose–Einstein parameters measured from various experiments.

the inner and the outer chamber are used. Pions are identified by their energy loss dE/dx. For all pion pairs Q^2_{BE} is calculated. To further increase the purity of the sample only $\pi^-\pi^-$ pairs are used for the like-pion spectrum, which then is compared to a reference spectrum constructed for $\pi^+\pi^-$ pairs. The ratio

$$\frac{N(Q^2_{BE}(\pi^-\pi^-))}{N(Q^2_{BE}(\pi^+\pi^-))} \quad \text{is fitted with the function} \quad R(Q^2_{BE}) = 1 + \lambda \exp(-\beta Q^2_{BE}) \quad (5)$$

Using unlike pairs as reference introduces a bias from the dynamics of the $\pi^+\pi^-$ spectrum. The region in Q^2_{BE} which corresponds to the mass of the K^0 and ρ^0 has been excluded (fig. 8 left). A smaller effect is expected from pairs, coming from $\eta-$, $\eta'-$ and $\omega-$ decays into three pions. A Monte Carlo study (Fig. 8) whithout BE effect

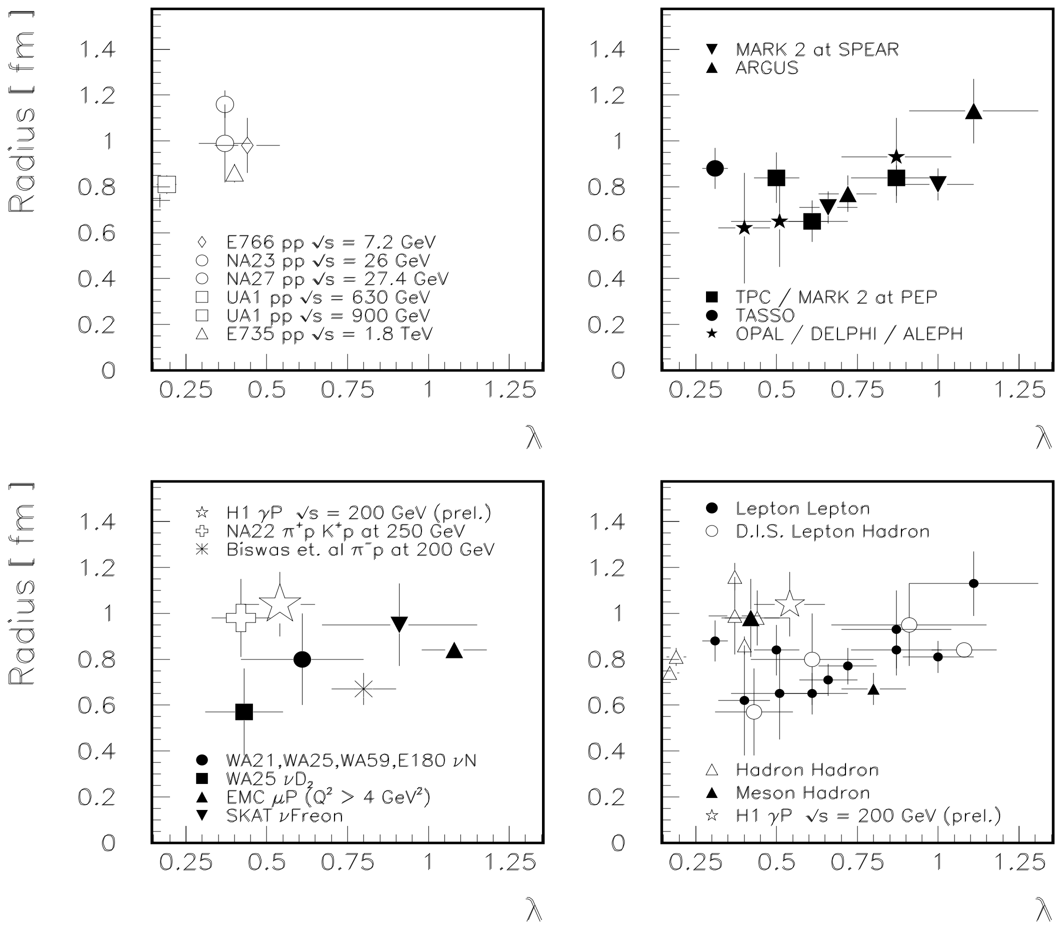

Figure 9: Bose Einstein Correlation for various experiments, see text

included proves that the pattern recognition introduces no bias. Only when the cut on long track is relaxed to tracks only starting in the inner chamber, the first bin shows an influence of the double track resolution. For the fit this bin (i.e. $Q^2_{BE} \leq 0.005GeV^2$) is excluded too. The systematic error is estimated from the fluctuations using different cuts on the tracks and the difference of the result in comparison to $\pi^+\pi^+$ pairs. The fit yields the values $r_{BE} = \hbar c\sqrt{\beta} = 0.197\sqrt{\beta} = 1.04 \pm 0.04_{stat} \pm 0.1_{sys}$ fm and $\lambda = 0.54 \pm 0.04_{stat} \pm 0.07_{sys}$.

In our comparison (Table 1) to other experiments we restricted ourselves to the gaussian ansatz for the Q^2_{BE} distribution with only small correction terms added in some cases. Figure 9 shows results from proton–proton (top left) electron–positron (top right) and meson–hadron or lepton–hadron (bottom left) scattering experiments. H1 observes a statistical correlation between the fitted parameters β and λ of +0.78, similar to the contour shape observed at LEP [46]. Therefore within large fluctuations one finds a clustering of the results into two groups near the pp and e^+e^- data. Parameters extracted from deep inelastic lepton–hadron scattering processes ([40] – [43]) seems to prefer the e^+e^- cluster while the recently measured meson–proton number [45] is close to the value observed from H1 for γp events. The similarity of the H1 measurement underlines once more the hadron like behavior of the photon.

4 Conclusions

Final state analysis of photoproduction events allow a classification of non perturbative processes and events to which an initial hard scattering of partons can be assigned. For the second class, kinematic variables of the partons can be extracted, thus leading to a structure measurement of the photon. At H1 the gluon content of the photon is observed. In the minimum bias photoproduction sample, events with large rapidity gaps are found. The gap arises for events where a colorless object, called Pomeron, is exchanged between the scattered hadrons. These diffractive events show a hard component too, which can lead to a structure analysis of the Pomeron.

Interference effects of final state pions in photoproduction events have been studied. A preliminary analysis in terms of the Goldhaber parametrisation and fit function yields values similar to those observed at meson–hadron collisions. The interesting question, whether this fragmentation parameters for highly virtual photon exchange are similar to the existing deep inelastic lepton hadron measurements will be answered with new data of increased statistics.

References

1. I.Abt *et al.*, H1 Collaboration, The H1 Detector at HERA, Desy preprint, DESY 93-103 (1993)
2. ZEUS Collaboration, The ZEUS Detector, Status report (1993)
3. F. Jacquet and A. Blondel, Proceedings of the Study for an ep Facility for Europe, ed. U. Amaldi, DESY 79/48 (1979) 133
4. I. Ahmed *et al.*, H1 Collaboration, Phys. Lett. **B299** (1993) 374
5. H. Bethe and W. Heitler, Proc. Roy. Soc. **A146** (1934) 83
6. I. Abt *et al.*, H1 Collaboration, Phys. Lett. **B338** (1994) 507
7. I. Abt *et al.*, H1 Collaboration, Phys. Lett. **B328** (1994) 176
8. G. Schuler and T. Sjöstrand, Phys. Rev. **D49** (1994) 2257
9. T. H. Bauer *et al.*, Rev. Mod. Phys 50 (1978) 261
10. B. A. Kniehl and G. Kramer Z. Phys. **C62** (1994) 53
11. I. Ahmed *et al.*, H1 Collaboration, Phys. Lett. **B297** (1992) 205
12. I. Ahmed *et al.*, H1 Collaboration, Phys. Lett. **B314** (1993) 436
13. J. E. Huth *et al.*, Fermilab–Conf–90/249-E(1990)
14. H. Bengtsson and T. Sjöstrand, Comp. Phys. Comm 46 (1987) 43
15. R. Akers *et al.*, OPAL Collaboration, Z. Phys. **C61** (1994) 199
16. R. Tanaka *et al.*, AMY Collaboration, Phys. Lett. **B277** (1992) 215
17. M. Glück, E. Reya and A. Vogt, Z. Phys. **C53** (1992) 651
18. H. Abramowicz, K. Charchula and A. Levy, Phys. Lett. **B269** (1991) 458
19. M. Derrick *et al.*, ZEUS Collaboration, Z. Phys. **C63** (1994) 391
20. I. Abt *et al.*,H1 Collaboration, DESY Desy preprint, DESY 94-198 (1994)
21. I. Pomeranchuk, Ya. JETP 7 (1958) 499
22. P. Bruni and G. Ingelman, Proceedings of the Europhysics Conference, Marseilles (1993) 595

23. J. Quebert, Ann. Phys. Fr 17 (1992) 99 and references cited herein
24. M. G. Bowler, Particle World 2 (1991) 1, ibid. Phys. Lett. **B180** (1986) 299
25. W. Zajc *et al.*, Phys. Rev. **C29** (1984) 1173
26. I. V . Andreev *et al.*, Phys. Rev. **D49** (1994) 1217
27. J. Bürger *et al.*, Nucl. Instr. and Meth. **A279** (1989) 217.
28. J. Uribe *et al.*, Phys. Rev. **D49** (1994) 4373
29. J. L. Bailly *et al.*, Z. Phys. **C43** (1989) 341
30. M. Aguilar-Benitez *et al.*, Z. Phys. **C54** (1992) 21
31. N. Neumeister *et al.*, Phys. Lett. B275 (1992) 186
32. T. Alexopoulos *et al.*, Phys. Rev. **D48** (1993) 1931
33. I. Jurici *et al.*, Phys. Rev. **D39** (1989) 1
34. G. Herrera, Proceedings of the XXII International Symposium on Multiparticle Dynamics, Santiago de Compostela, Spain 1992, p.69
35. H. Aihara *et al.*, Phys. Rev. **D31** (1985) 996
36. M. Althoff *et al.*, Z. Phys. **C29** (1985) 347
37. P. D. Acton *et al.*, Phys. Lett. **B267** (1991) 143
38. P. Abreu *et al.*, Phys. Lett. **B286** (1992) 201
39. D. Decamp *et al.*, Z. Phys. **C54** (1992) 75
40. V. A. Korotkov *et al.*, Z. Phys. **C60** (1993) 37
41. D. Allasia *et al.*, Z. Phys. **C37** (1988) 527
42. M. Arneado *et al.*, Z. Phys. **C32** (1986)
43. V. V. Ammasov *et al.*, Sov. J. Nucl. Phys. 53 (1991) 609
44. N. Biswas *et al.*, Phys. Rev. Lett. 37 (1976) 175
45. M. Adamus *et al.*, Z. Phys. **C37** (1988) 347
46. P. Abreu *et al.*, Phys. Lett. **B323** (1994) 242